DOI: 10.1111/cgf.14764
EUROGRAPHICS 2023 / K. Myszkowski and M. Nießner
(Guest Editors)

COMPUTER GRAPHICS *forum*
Volume 42 (2023), Number 2

Evolving Guide Subdivision

K. Karčiauskas[1] and J. Peters[2]

[1]Vilnius University [2] University of Florida

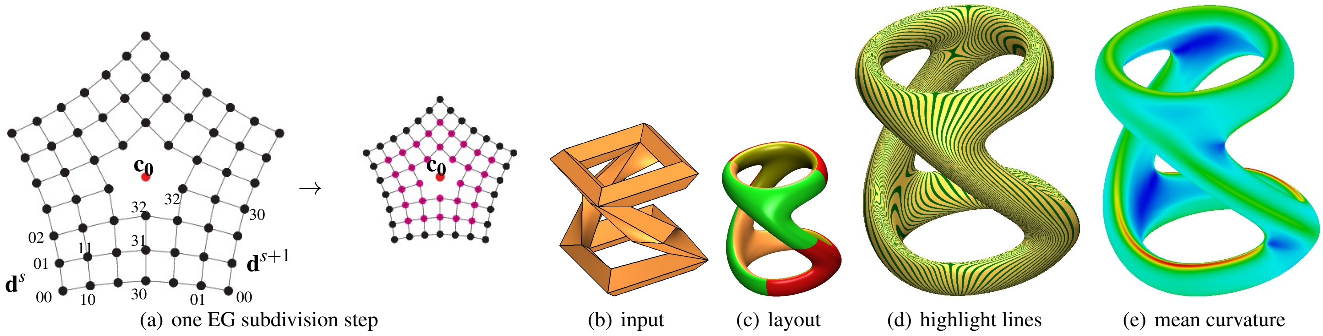

Figure 1: *EG subdivision. (a) Magenta bullets* • *have five tabulated rules (stencils applied using structural symmetry) in addition to the rule for the extraordinary point* $\mathbf{c_0}$*. (b) Un-symmetric input control net with* 8 *extraordinary nodes of valence* 6*. (c,d,e) The EG surface does not reveal the extraordinary points.*

Abstract

To overcome the well-known shape deficiencies of bi-cubic subdivision surfaces, Evolving Guide subdivision (EG subdivision) generalizes C^2 *bi-quartic (bi-4) splines that approximate a sequence of piecewise polynomial surface pieces near extraordinary points. Unlike guided subdivision, which achieves good shape by following a guide surface in a two-stage, geometry-dependent process, EG subdivision is defined by five new explicit subdivision rules. While formally only* C^1 *at extraordinary points, EG subdivision applied to an obstacle course of inputs generates surfaces without the oscillations and pinched highlight lines typical for Catmull-Clark subdivision. EG subdivision surfaces join* C^2 *with bi-3 surface pieces obtained by interpreting regular sub-nets as bi-cubic tensor-product splines and* C^2 *with adjacent EG surfaces. The EG subdivision control net surrounding an extraordinary node can have the same structure as Catmull-Clark subdivision: two rings of 4-sided facets around each extraordinary nodes so that extraordinary nodes are separated by at least one regular node.*

1. Introduction

In Catmull-Clark subdivision [CC78], except for extraordinary nodes, all new nodes of a refinement step are defined by regular bi-cubic (bi-3) uniform knot-insertion rules. (An extraordinary node is a mesh node that has fewer or more than the regular $n = 4$ neighbors.) The simplicity of just one special rule for each valence $n \neq 4$ makes implementation conceptually easy and broadly applicable (see e.g. [NLMD12] for a canonical implementation with additional features). However, the simple rules come at the cost of non-uniformly distributed highlight lines, e.g. visually unpleasant pinching of highlight lines near the extraordinary point, see Fig. 12e or Fig. 16f. Uniform highlight line distribution is a standard criterion for high surface quality [BC94] and the non-uniformity hints at the subdivision surface's inherent unbounded curvature in the limit. In response, Malcolm Sabin pioneered curvature-bounded subdivision [Sab91]. To control curvature at the limit extraordinary point $\mathbf{c_0}$, curvature-bounded subdivision has special refinement rules also for the $2n$ nearest neighbors of the extraordinary node. Initial versions of curvature-bounded subdivision resulted in undue flatness at the extraordinary point for convex control neighborhoods of the extraordinary node, [PU98]. Arguably the best shape of this class of 'tuned' subdivision algorithms is obtained by Ma-Ma subdivision surfaces [MM18] where, following [Sab91], each bi-3 patch of Catmull-Clark subdivision is replaced by 2×2 bi-3 macro-patches. The resulting shape is good, except for curvature oscillations at the transitions between the surface rings, see Fig. 12d,f. Also in the spirit of [Sab91], [LFS16] prescribe part of the Taylor expansion

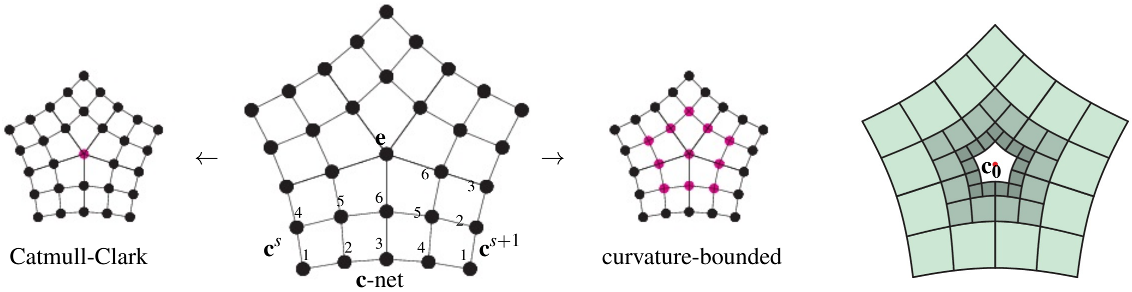

(a) bi-cubic subdivision net (b) contracting rings

Figure 2: *(a) Bi-3 subdivision algorithms using a* **c***-net as input. Magenta bullets (left and right of the* **c***-net) are obtained by special rules. (b) the standard layout of contracting subdivision surface rings.*

to prevent shape defects where the knot-spacing near the extraordinary point is highly unequal. Guided subdivision [KP18, KP19] provides a still more complete geometric Taylor expansion at the extraordinary point by making the subdivision surface follow an initially-computed, hence *static* guide surface. The shape of guided subdivision is reportedly very good, but guided subdivision is complex to implement due to its two construction stages: first construct the guide surface and then the subdivision surface, as a series of surface extension operators.

The contribution of the new EG subdivision algorithm is that it *achieves the surface quality of guided subdivision with the explicit formulas familiar from classical or tuned algorithms*. The number of output patches is the same as for Catmull-Clark subdivision and therefore $1/4$th of the tuned algorithms. Of course a price has to be paid: the polynomial degree of the surface near extraordinary points is increased to bi-quartic (bi-4) and generalizes bi-4 C^2 splines that smoothly join bi-3 C^2 splines of any surrounding regular quad-grid. That is, apart from where the extraordinary rules apply, the surface is the same uniform tensor-product bi-cubic spline as for Catmull-Clark subdivision. While Catmull-Clark subdivision has just one extraordinary rule, Ma-Ma subdivision has three (and 4 times as many bi-cubic pieces) and EG subdivision has five in addition to the once-executed rule for setting the limit point. On the other hand, the footprint of the EG rules is smaller than of guided subdivision. For example, the tight, not symmetric input control net Fig. 1b yields a surface consisting of eight 6-sided EG subdivision pieces that join directly, i.e. without requiring separating bi-3 surfaces generated from regular sub-nets, see Fig. 1c. This input net was chosen to rule out that the good shape is due to accidental symmetries and sufficiently small so that shape is not dominated by regular bi-cubic surfaces. The highlight lines in Fig. 1d are remarkably uniform and the mean curvature in Fig. 1e reveals neither unwanted oscillations nor betrays the locations of the extraordinary points. The key to this good shape is that EG subdivision follows an *evolving* converging sequence of piecewise polynomial surface caps baked into the explicit EG subdivision rules.

As input, EG subdivision requires only second-order Hermite boundary data and a central limit point $\mathbf{c_0}$. These can be obtained from a **c**-*net*, the control net of Catmull-Clark subdivision, i.e. two rings of quads surrounding a node of valence n with its direct and diagonal neighbor nodes of regular valence 4, see Fig. 2a. Alternatively, the control net of EG subdivision is a **d**-net: a **d**-*net* has the structure of a **c**-net with the central node removed and extended on the outside by one quad layer. All interior nodes have valence 4, see Fig. 1a. The nodes are interpreted as a C^2 bi-4 spline control points while the EG caps are of degree bi-4.

Overview After a review of recent progress in subdivision surface algorithms, Section 2 recalls the rules for regular C^2 bi-4 subdivision. Section 3 shows how **c**-nets are converted to **d**-nets and how to set the extraordinary point, $\mathbf{c_0}$. Section 4 contains the technical derivation of the rules of EG subdivision. This section can be skipped by the non-specialist. It is only intended for the specialist to follow the derivation. Section 5 presents the subdivision rules and Section 6 analyses the eigenstructure of the resulting limit surface. Examples and Discussion follow in Section 7. While Section 5 already presents explicit formulas (stencils) for $n = 3$ and $n = 5$, the formulas for valences $n = 6,7,8,9,10$ are provided in the Appendix.

1.1. Literature

Catmull-Clark subdivision [CC78] generalizes uniform bi-cubic (bi-3) tensor-product spline refinement to polyhedral control nets. Catmull-Clark subdivision is widely used in character animation [DKT98, NLMD12] and less so in industrial design [Ma05]. Repeated Catmull-Clark subdivision steps accumulate hyperbolic terms that result in geometric artifacts near extraordinary points whose valence is $n > 4$ [KPR04]. A number of algorithms, with increased complexity, have been devised to remedy this flaw in the limit, see e.g. [ADS06, CADS09, MM18, LFS16]. [CADS09, MM18] modify the differential expansion at the extraordinary point by adjusting subdivision weights; [LFS16] even prescribes leading parts of the eigenstructure. Guided Subdivision [KP07] removes artifacts by providing the limit differential expansion and eigenstructure directly and geometrically in the form of a guide surface. In all cases, this comes at the cost of more complex rules to generate the contracting subdivision surface rings. Subdivision rules have also been adjusted to improve convergence when used to solve partial differential equations [WLZH21, ZSC18].

The shape of EG subdivision surfaces is very similar to surfaces generated by the bi-4 variant of [KP19] that generalizes the approach in [KP18]. The best outcome among five compared variants

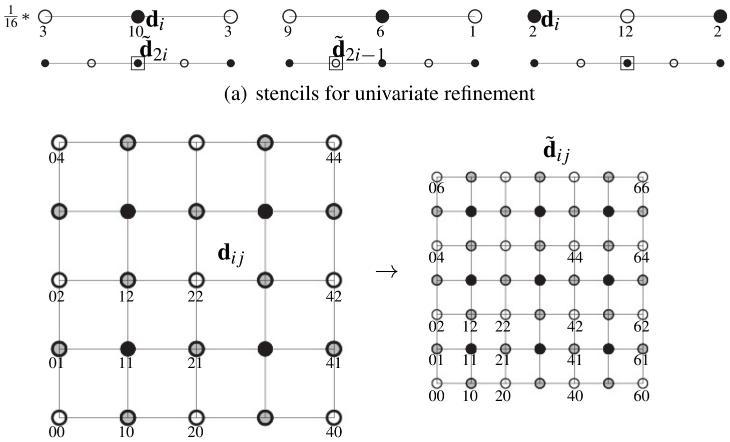

(a) stencils for univariate refinement

(b) two-dimensional refinement

Figure 3: *Refinement of degree 4 C^2 B-splines: (a) curve case; nodes (marked ○ are associated with simple knots, marked ● with double knots. (b) tensor-product bi-4 surface case.*

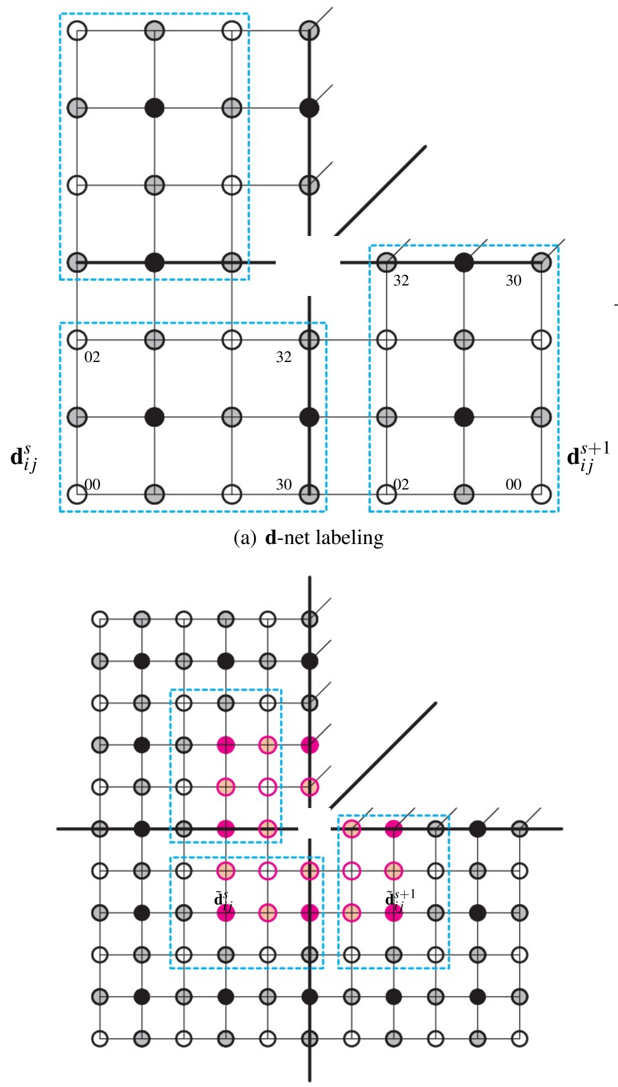

(a) **d**-net labeling

(b) **d**-net refinement

Figure 4: *Input and structure of EG subdivision: (a) input* **d***-net; no central point* $\mathbf{c_0}$*. (b) Regular rules ○, ●, ● and EG subdivision rules ●.*

of curvature-bounded guided subdivision is for a variant of degree bi-4 akin to EG subdivision. Both best constructions have bi-cubic variants that require more pieces and result in a slight deterioration of shape (see Fig. 21 and [KP19, Figs 2, 27]). The alikeness of shape is remarkable since the guided subdivision constructions in [KP19] and [KP18] yield excellent shape but are far more complicated: they require creating an explicit guide and a process of prolongation rather than the explicit formulas of EG subdivision.

Fig. 2a juxtaposes the nodes with special rules of bi-3 Catmull-Clark and Ma-Ma subdivision. These two algorithms are the main ones to be compared to since Catmull-Clark subdivision is widely used and [MM18] is the best of its class of 'tuned' bi-3 subdivision algorithms ([MM19] has a subdominant eigenvalue yielding faster contractions, but the oscillations increase). Both generate a sequence of C^2-connected C^2 contracting rings, see Fig. 2b. Each sector of a ring consists of Bézier patches, three for Catmull-Clark subdivision [CC78] and $3\times2\times2$ for Ma-Ma subdivision [MM18]. Since subdivision surfaces have to have a parameterization of degree at least bi-6 to yield C^2 surfaces [PR08], Catmull-Clark, Ma-Ma and EG subdivision can only be C^1 at the extraordinary point $\mathbf{c_0}$ (●).

2. C^2 bi-4 spline subdivision

We first recall the regular subdivision rules of tensor-product C^2 degree 4 splines (bi-4 splines) by knot insertion. The stencils for *univariate* refinement are shown in Fig. 3a. The stencils are convex combinations of the old nodes (top) and yield the three cases of new nodes that are indicated by □. Note that the stencil weights are always scaled to sum to 1. For example, the stencil on the left implies that a new point $\tilde{\mathbf{d}}_{2i}$ corresponding to an even-labeled old point $\mathbf{d}_i$ is obtained as an average of 10/16 the old point $\mathbf{d}_i$, and 3/16 times each of its old neighbors $\mathbf{d}_{i-1}$ and $\mathbf{d}_{i+1}$. For a new point $\tilde{\mathbf{d}}_{2i-1}$ to the left of $\mathbf{d}_{2i}$, the weights are 9/16, 6/16 and 1/16. Tensoring this univariate refinement yields nodes with simple knots (marked ○ in Fig. 3b), double knots (marked ●) in u and v, and single in one and double in the other variable (marked ●). The explicit formulas for the refinement of bi-4 C^2 B-splines, $\mathbf{d}\to\tilde{\mathbf{d}}$, are:

$$
\begin{aligned}
\mathbf{d} &:= \frac{1}{256}[\mathbf{d}_{00},\mathbf{d}_{10},\mathbf{d}_{20},\mathbf{d}_{30},\mathbf{d}_{01},\mathbf{d}_{11},\mathbf{d}_{21},\mathbf{d}_{31},\mathbf{d}_{02},\mathbf{d}_{12},\mathbf{d}_{22},\mathbf{d}_{32}]^T,\\
\tilde{\mathbf{d}}_{00} &:= [81,54,9,0,54,36,6,0,9,6,1,0]\mathbf{d},\\
\tilde{\mathbf{d}}_{10} &:= [27,90,27,0,18,60,18,0,3,10,3,0]\mathbf{d},\\
\tilde{\mathbf{d}}_{11} &:= [9,30,9,0,30,100,30,0,9,30,9,0]\mathbf{d},\\
\tilde{\mathbf{d}}_{30} &:= [0,18,108,18,0,12,72,12,0,2,12,2]\mathbf{d}, \qquad (1)\\
\tilde{\mathbf{d}}_{31} &:= [0,6,36,6,0,20,120,20,0,6,36,6]\mathbf{d},\\
\tilde{\mathbf{d}}_{33} &:= (36\mathbf{d}_{22}+6(\mathbf{d}_{21}+\mathbf{d}_{12}+\mathbf{d}_{32}+\mathbf{d}_{23})+\mathbf{d}_{11}+\mathbf{d}_{33}+\mathbf{d}_{31}+\mathbf{d}_{13})/64.
\end{aligned}
$$

The remaining $\tilde{\mathbf{d}}_{ij}$ are defined by symmetry as follows:
$\tilde{\mathbf{d}}_{01}$ is obtained from $\tilde{\mathbf{d}}_{10}$ replacing $\mathbf{d}_{ij}$ by $\mathbf{d}_{ji}$;
$\tilde{\mathbf{d}}_{2r}$, $r=0,1$, are obtained from $\tilde{\mathbf{d}}_{0r}$ replacing $\mathbf{d}_{ij}$ by $\mathbf{d}_{2-i,j}$;
$\tilde{\mathbf{d}}_{r2}$, $r=0,\dots,3$, are obtained from $\tilde{\mathbf{d}}_{r0}$ replacing $\mathbf{d}_{ij}$ by $\mathbf{d}_{i,2-j}$;
$\tilde{\mathbf{d}}_{r3}$, $r=0,1,2$, are obtained from $\tilde{\mathbf{d}}_{3r}$ replacing $\mathbf{d}_{ij}$ by $\mathbf{d}_{ji}$;
$\tilde{\mathbf{d}}_{r+4,s}$ are obtained from $\tilde{\mathbf{d}}_{rs}$ replacing $\mathbf{d}_{ij}$ by $\mathbf{d}_{2+i,j}$;
$\tilde{\mathbf{d}}_{r,s+4}$ are obtained from $\tilde{\mathbf{d}}_{rs}$ replacing $\mathbf{d}_{ij}$ by $\mathbf{d}_{i,2+j}$.

To extend the formulas to irregular multi-sided configurations we consider n groups of 12 nodes, see Fig. 4a:

$$\mathbf{d}^s_{ij}, \quad i=0,\dots,3, \quad j=0,\dots,2, \quad s=0,\dots,n-1. \tag{2}$$

The superscript s indicates a sector as marked by cyan dashed boxes. The configuration of n sectors is called a **d**-net. All but n nodes $\mathbf{d}^s_{32}$ of the **d**-net have valence 4 (are regular). The solid lines in Fig. 4a serve only to delineate the sectors and $\mathbf{d}^s_{32}$ has three neighbors. In particular, the intersection of the solid lines is not a control point.

Regular refinement yields the nodes marked •, ◦ or ● in Fig. 4b. The $6n$ magenta nodes depend on special rules to be derived and explained in Section 5. The refined net defines a surface ring of $3n$ polynomial pieces of degree bi-4 that matches the second-order Hermite data at the outer boundary of the ring and so is a C^2 prolongation. The nodes in cyan dashed boxes in Fig. 4b form a *refined* net with nodes denoted as $\tilde{\mathbf{d}}$. Each step yields a new C^2 bi-4 ring that is C^2-connected to the current bi-4 ring. Although formally C^2 and rather simple, a careful definition of new magenta nodes in Section 5 is key to obtaining good shape near the extraordinary point.

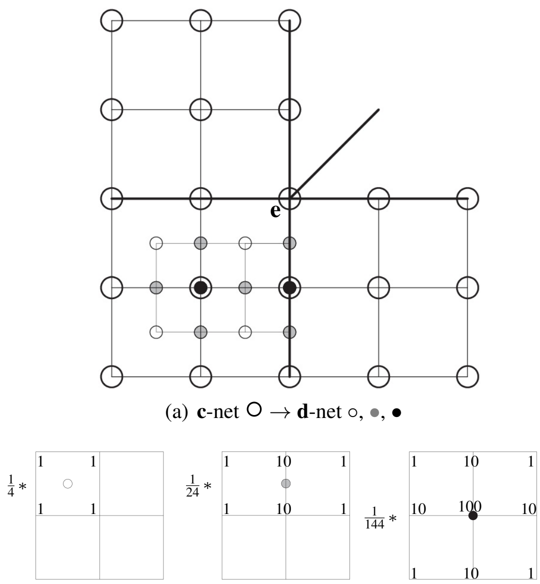

(a) **c**-net ○ → **d**-net ◦, ●, •

(b) stencils for 'degree-raising'

Figure 5: *'Degree-raising' a* **c***-net to a* **d***-net.*

3. Initialization: $\mathbf{c} \to \mathbf{d}$ and setting the limit point $\mathbf{c_0}$

If the input net is a **c**-net with extraordinary node **e**,

$$\mathbf{c_0} := \begin{cases} \frac{n}{n+5}\mathbf{e} + \frac{4}{n(n+5)}\sum_{i=0}^{n-1}\mathbf{c}^i_6 + \frac{1}{n(n+5)}\sum_{i=0}^{n-1}\mathbf{c}^i_5, & n>4,\\ \frac{11}{32}\mathbf{e} + \frac{1}{6}\sum_{i=0}^{n-1}\mathbf{c}^i_6 + \frac{5}{96}\sum_{i=0}^{n-1}\mathbf{c}^i_5, & n=3, \end{cases} \tag{3}$$

i.e. $\mathbf{c_0}$ is the extraordinary limit point of Catmull-Clark subdivision [HKD93], slightly corrected for $n=3$ as in [KP15].

We *degree-raise* the **c**-net to a **d**-net: $\mathbf{d} := \mathbf{R}\mathbf{c}$ where $\mathbf{R}$ is a $12n \times 6n+1$ matrix whose entries do not depend on n and that can be applied per sector, see Fig. 5: the **c**-net nodes are marked as ○ and the **d**-net nodes as •, ● or ◦. For one sector, Fig. 5b gives the degree-raising stencils that, in different positions, define 12 rows of **R**.

Conversely, when the input is a **d**-net and therefore lacks a central node, $\mathbf{c_0}$ is determined by fitting a **c**-net $\tilde{\mathbf{c}}$ (with $6n+1$ undetermined nodes) to **d**: apply the stencils of Fig. 5b to $\tilde{\mathbf{c}}$ and minimize the sum of squared distances between the corresponding nodes and **d**. Then $\mathbf{c_0}$ is defined by applying (3) to $\tilde{\mathbf{c}}$. For an input **d**-net, the explicit solution of this approach is

$$\mathbf{c_0} := \sum_{s=0}^{n-1}\sum_{i=0}^{3}\sum_{j=0}^{2}\frac{e_{ij}}{\gamma_n}\mathbf{d}^s_{ij}, \tag{4}$$

$$\begin{aligned} &e_{10} := -6e_{00}, e_{01} := e_{10},\ e_{02} := e_{20},\ e_{12} := e_{21}, e_{21} := -6e_{20},\\ &n>4: \gamma_n := 178480n(n+5); \quad \delta_n := 11185n(n+5);\\ &\qquad e_{20} := 19339n - 53929,\ e_{30} := 336(153n-448),\\ &\qquad e_{22} := 157051n + 50279,\ e_{32} := \frac{\gamma_n}{\delta_n}(8483n - 5008),\\ &\qquad e_{00} := 2587n - 8377, e_{11} := 36e_{00},\ e_{31} := -6e_{30},\\ &n=3: \gamma_3 := 93120, \quad e_{00} := 11,\ e_{20} := -73,\ e_{11} := 396,\\ &\qquad e_{22} := 10643,\ e_{32} := 19062,\ e_{30} := e_{10},\ e_{31} := e_{11}. \end{aligned}$$

4. Derivation of the refinement rules

This technical section is intended for the specialist to retrace the derivation of the subdivision rules and is not needed to use or implement EG subdivision. The steps are computed symbolically, not numerically, to yield the subdivision rules.

Since the subdivision surface is piecewise polynomial, the derivation takes advantage of the Bernstein-Bézier form (BB-form, [dB87, Far88]). For Bernstein polynomials $B^d_k(t) := \binom{d}{k}(1-t)^{d-k}t^k$ the polynomials of bi-degree $d=4$ are

$$\sum_{i=0}^{d}\sum_{j=0}^{d}\mathbf{b}_{ij}B^d_i(u)B^d_j(v), \quad 0 \le u,v \le 1.$$

Connecting the *BB-coefficients* $\mathbf{b}_{ij} \in \mathbb{R}^3$ to $\mathbf{b}_{i+1,j}$ and $\mathbf{b}_{i,j+1}$, wherever well-defined, yields the *BB-net*.

To express C^2 degree $d=4$ splines in BB-form, we first consider one variable. Every even-labeled spline control point $\mathbf{d}_{2s}$, marked ◦ in Fig. 6a, is associated with a single knot and is interpreted as the middle BB-coefficient of a corresponding curve segment with label s, i.e. $\mathbf{b}^s_2 := \mathbf{d}_{2s}$. Every odd-labeled control point (labeled $\mathbf{d}_{2s-1}$ and marked • in Fig. 6a) is associated with a double knot and corresponds to, but is typically not equal to, the common BB-coefficient

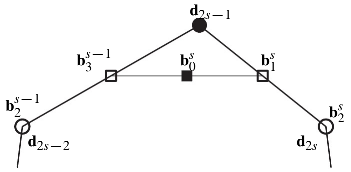

(a) univariate degree 4 B-to-BB conversion

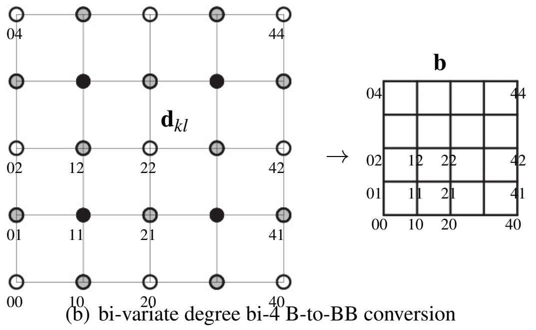

(b) bi-variate degree bi-4 B-to-BB conversion

Figure 6: *Conversion from degree* 4 C^2 *B-spline form to BB-form: (a) univariate case; (b) tensor-product case. The four* $\mathbf{d}_{kl}$ *marked by* • *correspond to corner coefficients* $\mathbf{b}_{00}$*,* $\mathbf{b}_{40}$*,* $\mathbf{b}_{44}$*,* $\mathbf{b}_{04}$ *of the bi-4 patch* $\mathbf{b}$*.*

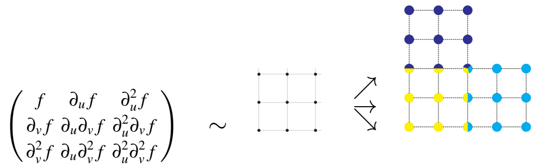

Figure 7: *Assembly of three corner jets into an L-net*

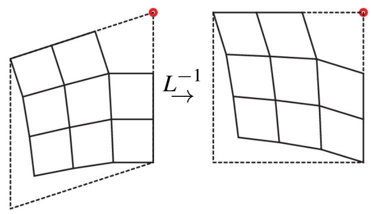

(a) linear transformation L

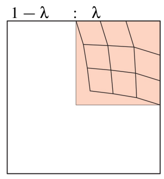

(b) sampling

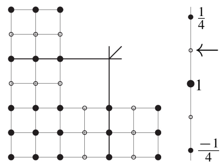

(c) C^2 correction

Figure 8: *Contraction of spline rings.*

of two curve segments $\mathbf{b}_4^{s-1} = \mathbf{b}_0^s$. The explicit formulas of the conversion to the BB-coefficients of segment s are:

$$\mathbf{b}_0^s := \frac{1}{4}(\mathbf{d}_{2s-2} + 2\mathbf{d}_{2s-1} + \mathbf{d}_{2s}),\ \mathbf{b}_4^s := \frac{1}{4}(\mathbf{d}_{2s} + 2\mathbf{d}_{2s+1} + \mathbf{d}_{2s+2}),$$
$$\mathbf{b}_1^s := \frac{1}{2}(\mathbf{d}_{2s-1} + \mathbf{d}_{2s}), \quad \mathbf{b}_2^s := \mathbf{d}_{2s}, \quad \mathbf{b}_3^s := \frac{1}{2}(\mathbf{d}_{2s} + \mathbf{d}_{2s+1}). \quad (5)$$

Tensoring the univariate case yields nodes with simple knots (marked ○ in Fig. 6b,*left*), double knots (marked •) in u and v and single in one and double in the other variable (marked •). The formulas for B-to-BB conversion, $\mathbf{d} \to \mathbf{b}$, are

$$\mathbf{d} := [\mathbf{d}_{00}, \mathbf{d}_{10}, \mathbf{d}_{01}, \mathbf{d}_{20}, \mathbf{d}_{02}, \mathbf{d}_{11}, \mathbf{d}_{21}, \mathbf{d}_{12}, \mathbf{d}_{22}]^T,$$
$$\mathbf{b}_{00} := \frac{1}{16}[1,2,2,1,1,4,2,2,1]\mathbf{d} \quad \mathbf{b}_{10} := \frac{1}{16}[0,2,0,2,0,4,4,2,2]\mathbf{d}$$
$$\mathbf{b}_{20} := (\mathbf{d}_{20} + 2\mathbf{d}_{21} + \mathbf{d}_{22})/4, \quad \mathbf{b}_{21} := (\mathbf{d}_{12} + \mathbf{d}_{22})/2, \qquad (6)$$
$$\mathbf{b}_{11} := (\mathbf{d}_{11} + \mathbf{d}_{21} + \mathbf{d}_{12} + \mathbf{d}_{22})/4, \quad \mathbf{b}_{22} := \mathbf{d}_{22}.$$

The remaining BB-coefficients are defined by symmetries: $\mathbf{b}_{01}$, $\mathbf{b}_{02}$, $\mathbf{b}_{12}$ are obtained from $\mathbf{b}_{10}$, $\mathbf{b}_{20}$, $\mathbf{b}_{21}$ by replacing $\mathbf{d}_{kl}$ by $\mathbf{d}_{lk}$; $\mathbf{b}_{kl}$, $k = 3,4$, $l = 0,1,2$ are obtained from $\mathbf{b}_{4-k,l}$ by replacing $\mathbf{d}_{kl}$ by $\mathbf{d}_{4-k,l}$; $\mathbf{b}_{kl}$, $k = 0,\dots,4$, $l = 3,4$ are obtained from $\mathbf{b}_{k,4-l}$ by replacing $\mathbf{d}_{kl}$ by $\mathbf{d}_{k,4-l}$. Analogous to $\mathbf{c}$-net conversion, conversion of the $\mathbf{d}$-net to BB-form (6) provides second-order Hermite data around the hole.

The construction repeatedly uses Taylor expansions, or *jets*, at corners of patches and Taylor expansions along boundaries of patches, called *tensor-borders*. For example, the second-order Taylor expansion of a map f at corner of its unit square domain can be collected in the matrix of partial derivatives at a corner point, see Fig. 7, *l*eft, that is re-expressed as a 3×3 BB-net (*r*ight of $\sim$) of some degree bi-d. Three corner jets (cyan,yellow and blue) can be merged into an L-net by averaging the BB-coefficients at overlapping locations. The L-net defines two tensor-borders of degree bi-4.

Let L be the linear transformation that maps the unit square into a unit-edge-length parallelogram with opening angle $\frac{2\pi}{n}$. Let χ be the characteristic map of Catmull-Clark subdivision with subdominant eigenvalue λ, see Fig. 8a. Scaling $\chi^T := L^{-1} \circ \chi$ by λ therefore maps the tensor-border of the characteristic map into the upper right pink area in Fig. 8b. Analogous to the construction for a $\mathbf{c}$-net, in [KP18, Appendix], we construct a map $\mathbf{g}$, consisting of n G^1-connected bi-5 sectors with a unique quadratic expansion at the common point, as an affine combination of the nodes $\mathbf{d}$ and $\mathbf{c_0}$. Restricting $\mathbf{g}$ to the same subdomain as χ^T therefore allows sampling the L-shaped bi-4 tensor-borders from $\mathbf{g} \circ \lambda\chi^T$, see Fig. 8c. These adjacent L-shaped pieces are off-hand C^1-connected, but applying the univariate stencil of Fig. 8c,*right* to ○ ← and its ○ sibling below by symmetry, makes the layers join C^2. Then we apply the inverse of the formulas (6), to yield $\mathbf{d}$ in terms of $\mathbf{b}$, to the n C^2-connected bi-4 tensor-borders. This defines the refined nodes $\tilde{\mathbf{d}}_{ij}^s$, $i = 0,\dots,3$, $j = 0,\dots,2$, $s = 0,\dots,n-1$.

In all sectors, $\tilde{\mathbf{d}}_{i0}^s$, $i = 0,\dots,3$, $\tilde{\mathbf{d}}_{0j}^s$, $j = 1,2$, are obtained by regular refinement of $\mathbf{d}$, see Fig. 4b. All calculations are symbolic and yield explicit affine expressions, shown in the next section, of the refined nodes $\tilde{\mathbf{d}}$ in terms of the initial nodes $\mathbf{d}$ and the central point $\mathbf{c_0}$ fixed in Section 3. Tabulating, for each valence n, the expressions in a subdivision matrix, respectively the arrays A_{ij}^n of Section 5 and the Appendix, completes the derivation of the algorithm.

5. The subdivision algorithm $\mathbf{d} \to \tilde{\mathbf{d}}$

The derivation in the previous section may give the impression that EG subdivision is complicated to implement. However implementation requires only five special rules in addition to rule (3), respectively (4) for $\mathbf{c_0}$. These rules, expressed as integer weights after scaling by 10^5, are presented here and in the Appendix. The six outer new nodes $\tilde{\mathbf{d}}^s_{hk}$ (for $h = 0$ or $k = 0$) are generated by the regular refinement rules (1). The six inner new nodes $\tilde{\mathbf{d}}^s_{hk}$, $h = 1,2,3,\ k = 1,2$, are each calculated by the following formula

$$\tilde{\mathbf{d}}^s_{hk} := a^{hk}_0 \mathbf{c_0} + \sum_{r=0}^{n-1} \sum_{i=0}^{3} \sum_{j=0}^{2} a^{r,hk}_{ij} \mathbf{d}^{s+r}_{ij}. \tag{7}$$

The pseudocode for EG is then (cf. `EGRefinePatchConstructor` in [LKP22])

> Prior to runtime, once ever:
> - for each valence n, assemble the subdivision matrix $\mathbf{A}_n$ by copying and replicating the 5-digit array entries $a^{r,hk}_{ij}$ using the structural symmetries explained below and extending to a full **d**-net by regular refinement (1).
>
> If input is a **d**-net
> - Set $\mathbf{c_0} \leftarrow \mathbf{d}$ by (4),
>
> If input is a **c**-net
> - if extraordinary nodes not separated by one regular node, apply one (local) Catmull-Clark subdivision step;
> - Set $\mathbf{d} := \mathbf{R}\mathbf{c}$, $\quad \mathbf{c_0} \leftarrow \mathbf{c}$ by (3).
>
> Repeat (subdivision step)
>
> Collect the **d**-net and the limit point $\mathbf{c_0}$ into $(\mathbf{d}, \mathbf{c_0})$, a $12n+1$ vector of points.
> - (output) Convert the **d**-net to a surface ring in BB-form by tensoring (5) or applying (6).
> - Then the new **d**-net points are
>
> $$(\mathbf{d}, \mathbf{c_0})^{\text{new}} := \mathbf{A}_n \cdot (\mathbf{d}, \mathbf{c_0})$$
>
> where $\cdot$ denotes matrix-vector multiplication.

The outer surface ring refined by regular rules (1) together with the new $\tilde{\mathbf{d}}$-net then define a C^2-joined bi-4 spline ring, that can be expressed in BB-form by the expressions (6).

All regular sub-nets of the input mesh can be interpreted as bi-3 C^2 B-spline control nets. The resulting bi-3 surface pieces join C^2 with the bi-4 EG surface caps because second-order Hermite data along the boundary of the EG subdivision pieces stems from degree-raised bi-3 uniform B-spline pieces generated when deriving the **d**-net from a **c**-net in Section 3. By the same reasoning abutting EG surface pieces join C^2.

It remains to specify the weights $a^{r,hk}_{ij}$. To have a partition of unity, the weight scaling the $\mathbf{c_0}$ contribution is $a^{hk}_0 := 1 - \sum_{r=0}^{n-1} \sum_{i=0}^{3} \sum_{j=0}^{2} a^{r,hk}_{ij}$. The inner double summation, whose indices are illustrated in Fig. 4a, is unfolded into a 4×3 vector with indices
00 10 20 30 01 11 21 31 02 12 22 32
to form the rows of each of the five arrays $A^n_{11}, A^n_{22}, A^n_{21}, A^n_{31}, A^n_{32}$ required to build $\mathbf{A}_n$. Here the superscript n is the valence and the subscript is the index of the new node.

Several symmetries, in the construction (not the geometry), simplify the formulas. For example, the rules for $\tilde{\mathbf{d}}^s_{12}$ follow from those of $\tilde{\mathbf{d}}^s_{21}$ by subscript exchange. Formula (7) clearly shows the rotational invariance of the construction. Mirror symmetries with respect to sector diagonals and sector separating lines imply further relations that allow shortening the arrays A^n_{hk} of precalculated weights $a^{r,hk}_{ij}$ (superscript '3' indicates nodes on the sector-separating line):

$$a^{r,hk}_{ij} = a^{-r,kh}_{ji},\ h = 1,2,\ k = 1,2, \qquad a^{r,3k}_{ij} = a^{-r+1,3k}_{ji},\ k = 1,2,$$
$$a^{r,hk}_{3j} = a^{-r-1,kh}_{3j},\ h = 1,2,\ k = 1,2, \qquad a^{r,3k}_{3j} = a^{-r,3k}_{3j},\ k = 1,2.$$

Therefore it suffices to list the full set of rows, i.e. $r = 0,\dots,n-1$, for only the new node with index 21. For $hk \in \{11,22\}$, we need only $r = 0,\dots,N$, where $N := \lfloor \frac{n}{2} \rfloor$, i.e. $N = 3$ for $n \in \{6,7\}$. For $hk \in \{31,32\}$, $r = 0,\dots,M$ where $M := \lfloor \frac{n+1}{2} \rfloor$, i.e. $M = 4$ for $n \in \{7,8\}$. The formulas have yet more symmetries, but some redundancy simplifies reading and implementation.

The formulas were initially computed with 20-digit accuracy, but truncating to 5 digits after the decimal point preserves good highlight line distributions. After scaling by 10^5, truncation allows us to explicitly list the $a^{r,hk}_{ij}$ as integers. Note that these integers are not approximations but are the exact EG subdivision rules. The integer representation facilitates an exact computation of the characteristic polynomial of the EG subdivision matrix. The arrays for $n = 6,7,8,9,10$ are listed in the Appendix and for $n = 3$ and $n = 5$ here. As an example of how to read the arrays below, see A^5_{11}: $a^{0,11}_{00} := -0.00129$, $a^{0,11}_{11} := 0.02629$ $a^{1,11}_{21} := -0.00111$ and $a^{2,11}_{30} := 0.00021$.

For $n = 3$,

$$A^3_{11} := \begin{pmatrix} -1 & -13 & -37 & 42 & -13 & 1671 & 10243 & 2049 & -37 & 10243 & 50096 & 5073 \\ 0 & 0 & 38 & 35 & -4 & 20 & -169 & -859 & -77 & -272 & -1886 & -2793 \end{pmatrix}$$
$$A^3_{22} := \begin{pmatrix} 0 & 6 & -49 & -96 & 6 & -87 & 2309 & 1776 & -49 & 2309 & 15760 & 6979 \\ 0 & 0 & 87 & 57 & -11 & 39 & -330 & -1928 & -58 & -793 & -3253 & -5925 \end{pmatrix}$$
$$A^3_{21} := \begin{pmatrix} 0 & -10 & 2 & 1 & -5 & 153 & 8101 & 7372 & -173 & 2036 & 32183 & 20229 \\ 0 & 3 & 46 & -11 & -7 & -3 & 98 & -966 & -118 & 328 & 1736 & -2329 \\ 0 & -8 & -3 & -128 & 0 & 16 & -709 & 307 & 55 & -198 & -2703 & 4434 \end{pmatrix}$$
$$A^3_{31} := \begin{pmatrix} 0 & -3 & 0 & 76 & 16 & -125 & 3642 & 9873 & 79 & -370 & 4902 & 23927 \\ 0 & 16 & 79 & 79 & -3 & -125 & -370 & -1761 & 0 & 3642 & 4902 & -6789 \\ ,0 & -7 & 113 & 79 & -7 & 80 & -1088 & -1761 & 113 & -1088 & -6828 & -6789 \end{pmatrix}$$
$$A^3_{32} := \begin{pmatrix} 0 & -3 & -30 & 63 & 9 & -28 & 792 & 2658 & 14 & -402 & 341 & 7126 \\ 0 & 9 & 14 & 44 & -3 & -28 & -402 & -1866 & -30 & 792 & 341 & -6175 \\ 0 & -4 & 63 & 44 & -4 & 62 & -1112 & -1866 & 63 & -1112 & -6536 & -6175 \end{pmatrix}$$

For $n = 5$,

$$A^5_{11} := \begin{pmatrix} -129 & 221 & 50 & -28 & 221 & 2629 & 6368 & 2877 & 50 & 6368 & 61638 & 6916 \\ -26 & 68 & -27 & 2 & 36 & -65 & -111 & -16 & 2 & -177 & -10 & -388 \\ 28 & -41 & -27 & 21 & -57 & -73 & 278 & -17 & 4 & 306 & -692 & -676 \end{pmatrix}$$
$$A^5_{22} := \begin{pmatrix} -491 & 973 & 57 & -205 & 973 & -322 & -4931 & 1147 & 57 & -4931 & 41825 & 11869 \\ -74 & 217 & -103 & 27 & 68 & -164 & -225 & -200 & 76 & -94 & 2039 & -3059 \\ 165 & -264 & -112 & 114 & -332 & -210 & 1422 & -150 & 34 & 1591 & -5064 & -3801 \end{pmatrix}$$
$$A^5_{21} := \begin{pmatrix} -256 & 482 & 14 & -132 & 582 & -379 & 5085 & 5035 & 70 & -3009 & 48736 & 23656 \\ -143 & 317 & -74 & -16 & 243 & -143 & -857 & -44 & -67 & 434 & 5702 & -564 \\ 89 & -140 & -48 & 53 & -195 & -107 & 773 & -48 & 67 & 874 & -2602 & -1630 \\ 57 & -96 & -42 & 35 & -83 & -172 & 625 & -107 & -74 & 552 & -1421 & -2015 \\ 49 & -135 & 104 & -135 & -59 & -88 & 456 & 957 & -37 & 538 & -1701 & 3402 \end{pmatrix}$$
$$A^5_{31} := \begin{pmatrix} -269 & 492 & -13 & -197 & 541 & -115 & -84 & 9355 & -192 & -1203 & 16754 & 43563 \\ -269 & 541 & -192 & -10 & 492 & -115 & -1203 & -313 & -13 & -84 & 16754 & 641 \\ 103 & -154 & -54 & 62 & -243 & -113 & 944 & -117 & 118 & 951 & -2635 & -2601 \\ 79 & -125 & -80 & 62 & -125 & -219 & 800 & -117 & -80 & 800 & -2081 & -2601 \end{pmatrix}$$
$$A^5_{32} := \begin{pmatrix} -433 & 772 & -48 & -208 & 910 & -235 & -3106 & 1327 & -264 & -2342 & 12285 & 25197 \\ -433 & 910 & -264 & -41 & 772 & -235 & -2342 & -207 & -48 & -3106 & 12285 & -542 \\ 220 & -354 & -73 & 125 & -509 & -69 & 1859 & -299 & 263 & 1600 & -6314 & -5478 \\ 169 & -285 & -124 & 125 & -285 & -260 & 1544 & -299 & -124 & 1544 & -5418 & -5478 \end{pmatrix}$$

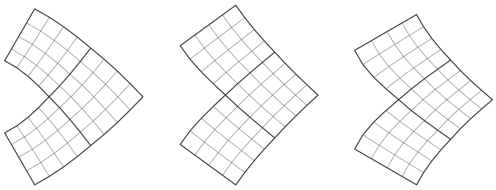

(a) $n=3$ (b) $n=5$ (c) $n=6$

Figure 9: *Characteristic map of EG subdivision (one sector).*

6. Limit Analysis

The eigenvalues of the $(12n+1)\times(12n+1)$ subdivision matrix can be computed directly by the software *Maple* based on the arrays A^n_{hk}. The discrete Fourier transform needs not be used. As expected, exactly one eigenvalue dominates and is 1, and $\mathbf{c_0}$ is the corresponding extraordinary point. The double subdominant eigenvalue λ differs from that of Catmull-Clark subdivision by less than 10^{-3} for any $n \geq 3$. This too is expected, since a linear transformation of the tensor-border of the characteristic map (ring) of Catmull-Clark subdivision was used to derive the refinement rules. With μ the subsubdominant eigenvalue, the deviation of $\frac{\mu}{\lambda^2}$ from 1 is small:

$n=$	3	5	6	7	8	9	10
$\frac{\mu}{\lambda^2}=$	1.00015	1.00016	1.00151	1.00241	1.02887	1.04865	1.05815

This is a consequence of the guide-based derivation of the refinement rules. The BB-nets of the characteristic rings, computed numerically for n=3,5,…,10, look identical (but are not identical) to those of the degree-raised characteristic maps of Catmull-Clark subdivision. Standard formal numerical computation confirms injectivity of the rings. Fig. 9 displays the characteristic maps for $n=3,5,6$.

7. Examples and Discussion

In the following examples, wherever a sub-net is regular, the control net is interpreted as a bi-3 tensor-product spline, just as for Catmull-Clark and Ma-Ma subdivision. The extraordinary nodes are assumed to be surrounded by a **c**-net and each **c**-net is 'degree-raised' to a **d**-net according to Section 3. Then the bi-4 EG surface joins C^2 with any bi-3 surface on the regular net and to neighboring EG surfaces. In the following examples, the input is a **c**-net extended by one ring of quads to define a surrounding bi-3 surface and so evaluate the transition from a regular bi-3 B-spline surface (green) to the bi-4 EG subdivision surface (reddish gold). An extended **c**-net is anyhow required to start curvature-bounded subdivision like Ma-Ma, because their rules have a larger support than those for Catmull-Clark subdivision. (If the surface not governed by the **c**-net is to be preserved, one Catmull-Clark-step needs to precede the first Ma-Ma step).

We focus on the shape of the non-regular caps where the surface differs from the uniform tensor-product bi-cubic spline surface. Small nets are preferred to assess shape over large 'real-life' meshes where regular surfaces dominate. As the egg cup in Fig. 10 illustrates, even for models of moderate size still-images from afar make it tricky to spot surface flaws evident under zoom

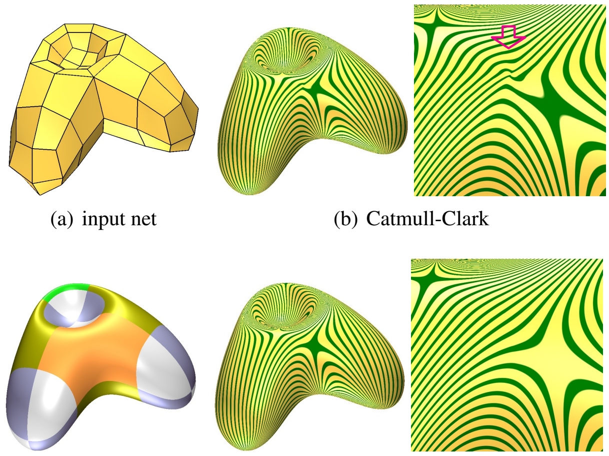

(a) input net (b) Catmull-Clark

(c) layout (d) EG subdivision

Figure 10: *Surfaces viewed from afar obscure shape deficiencies.*

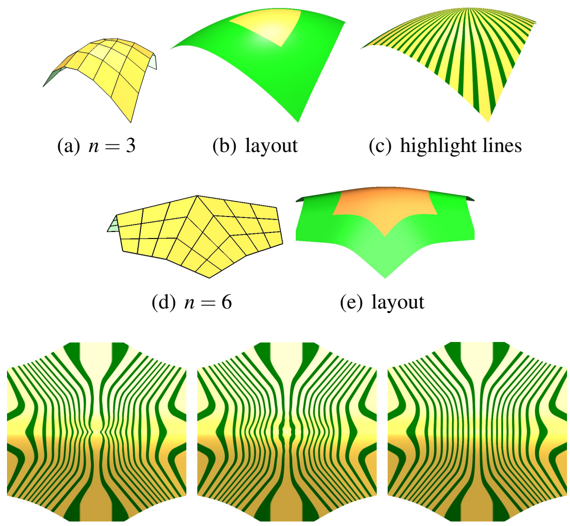

(a) $n=3$ (b) layout (c) highlight lines

(d) $n=6$ (e) layout

(f) Catmull-Clark (g) Ma-Ma (h) EG

Figure 11: *Convex shapes for $n=3$ and $n=6$.*

(*r*ight) or when interactively moving the object. The following small, carefully-selected examples enable shape prediction and surface quality verification.

Fig. 11 tests the new algorithm for convex input nets. For $n=3$, often an outlier in terms of shape, the highlight line distribution is uniform. Fig. 11d consists of 6 planar sectors tangent to a slightly bent cylinder. Catmull-Clark and Ma-Ma exhibit oscillations near the extraordinary point, while EG subdivision does not. The input of Fig. 12 are 7 planar sectors to be blended. The highlight lines of eight subdivision rings show pinching for Catmull-Clark subdivision in Fig. 12e. Ma-Ma subdivision applied to the extended **c**-net shows unexpected kinks in the highlight lines, see ⇧ in Fig. 12c. Unlike Catmull-Clark, Ma-Ma does not preserve the in-

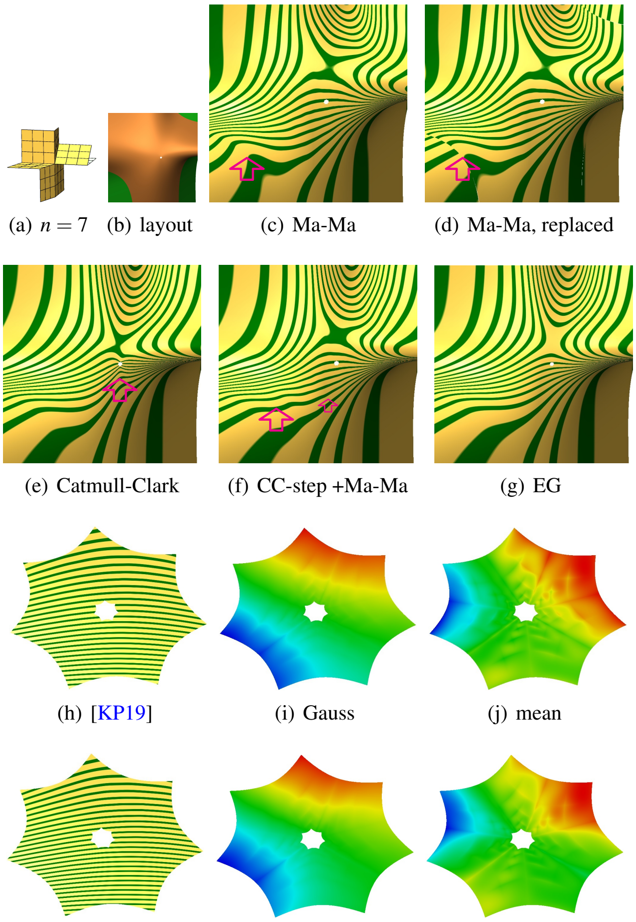

(a) $n=7$ (b) layout (c) Ma-Ma (d) Ma-Ma, replaced

(e) Catmull-Clark (f) CC-step +Ma-Ma (g) EG

(h) [KP19] (i) Gauss (j) mean

(k) EG (l) Gauss (m) mean

Figure 12: *Blending 7 planar sectors. (c) applying [MM18] to the extended* **c***-net yields sharp turns, (d) replacing the outermost ring with a Catmull-Clark (CC) ring results in a discontinuity, (e) CC yields pinched highlight lines near the center. (f) prepending one step of CC moves smaller ripples inwards. (h–m) zoom on the inner four of nine rings of [KP19] vs. EG subdivision reveal strong similarity in highlight lines, Gauss and mean curvature.*

put ring. This results in gaps when the first ring is replaced by the bi-3 ring of the **c**-net extension as illustrated in Fig. 12d. Therefore one Catmull-Clark refinement step must be applied before starting Ma-Ma subdivision. The ripples in the resulting surface become milder than those in Fig. 12c but they repeat inwards, see Fig. 12f. By contrast, for EG the highlight line distribution is nearly uniform, see Fig. 12g. As aimed for, to spot any difference between EG subdivision and [KP19] requires zooming in on the last four of nine surface rings. The bottom two rows of Fig. 12 reveal slight differences in curvature, expected due to the different initial guide and the fact that the baked-in guide of EG subdivision evolves with refinement. Despite the differences, no case can be made that one surface shape is superior to the other.

To obtain a finite construction, the hole remaining after k steps of subdivision can be filled with a multi-sided cap. Fig. 13 illustrates the use of a bi-4 G^1 cap in the spirit of [KP19]. Fig. 13a is considered a difficult input net since some consecutive sectors are co-planar. Here the EG subdivision is capped after 8 rings. The highlight lines are well-distributed both in the large, see Fig. 13c, and when zooming in, see Fig. 13e. Though formally only G^1, Fig. 13e,f demonstrate high quality also of capped EG subdivision. Fig. 14a models a two-beam corner using $n=5$. A bi-4 cap fills the hole after 3 rings. The highlight lines in Fig. 14c are well-distributed.

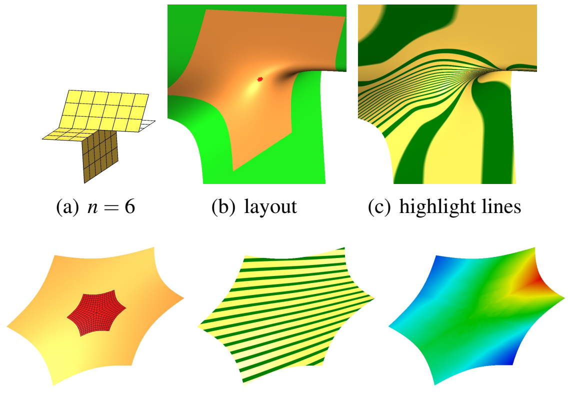

(a) $n=6$ (b) layout (c) highlight lines

(d) BB-net of cap (e) highlight lines (f) mean curvature

Figure 13: *Blending 4 planar faces and filling the hole. Surface layout: surrounding bi-3 surface, 8 rings of subdivision surface and tiny G^1 bi-4 cap with 2×2 sectors (see (d)). bottom: last 3 rings + tiny cap.*

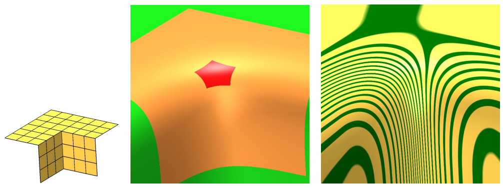

(a) $n=5$ (b) layout (c) highlight lines

Figure 14: *Blending 3 planes, $n=5$. Surface layout: surrounding bi-3 surface, three subdivision surface rings and G^1 bi-4 cap.*

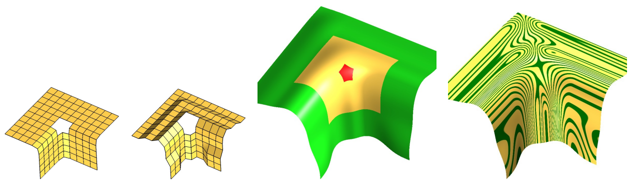

(a) (b) (c) layout (d) highlight lines

Figure 15: *(a) Net 'degree-raised' from Fig. 14 and (b) its perturbation to insert grooves along the top plane and the upward blend.*

Fig. 15 demonstrates the insertion of grooves into the two-beam corner of Fig. 14. The extended **c**-net is 'degree-raised', i.e. the stencils of Fig. 5 are applied wherever well-defined. Then the **d**-net appears as the interior sub-net. The entire new net is perturbed to yield the groves. Fig. 16 rounds the beams of a regular oc-

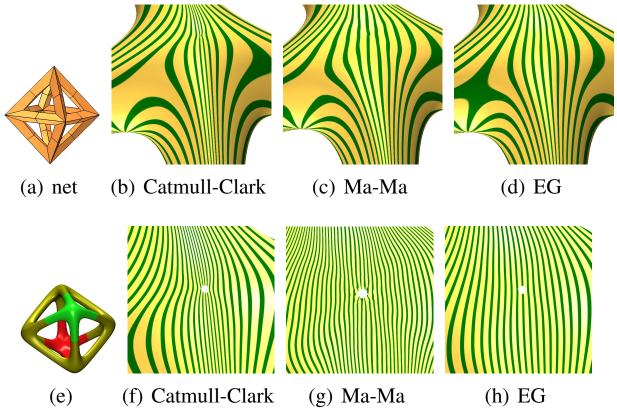

Figure 16: *Octahedral beam net. (b,c,d): green part of (e); (f,g,h): zoom to rings 3 to 9.*

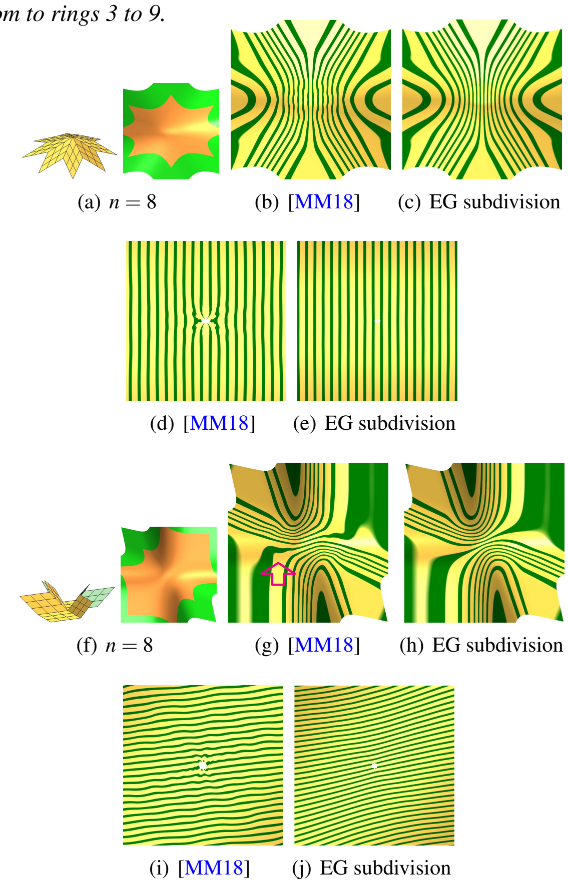

Figure 17: *Convex net and saddle net for $n = 8$: comparison of transition (first ring) and limit shape.*

tahedron scaffold (a). The scaffold contains 12 nodes of valence

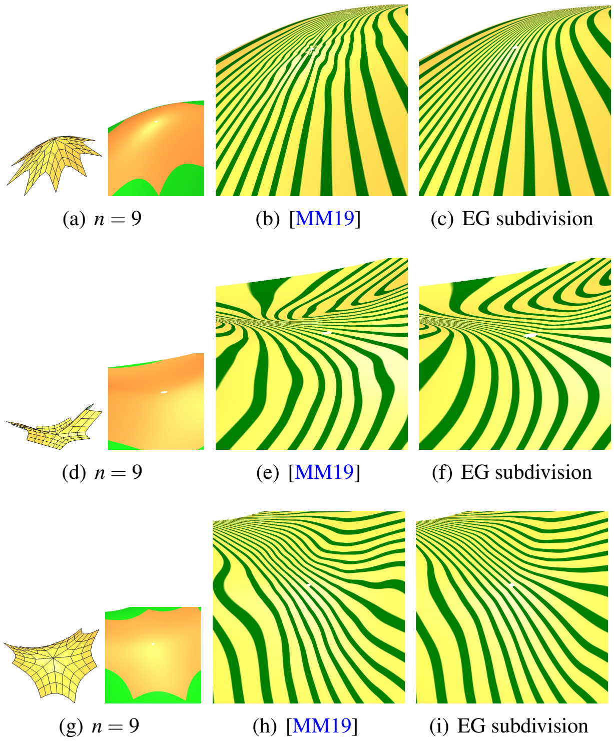

Figure 18: *$n = 9$ extended* **c***-nets*

8. While the pinched highlight lines of the Catmull-Clark surface in (b) reveal high curvature near the extraordinary point, and (c) Ma-Ma surfaces [MM18] have fine oscillations, the highlight line distribution of EG subdivision is remarkably uniform. The magnification in the second row reveals artifacts that a designer would flag. Under zoom, we see that for a convex input net, Catmull-Clark subdivision concentrates the artifacts near the limit point while Ma-Ma [MM18] spreads them out. Elaborating on the flaws of Catmull-Clark and Ma-Ma in Fig. 16, the **c**-nets of Fig. 17 illustrate, for convex and saddle inputs, the advantages of EG subdivision. The artifacts of Ma-Ma concentrate at the first ring transition (Fig. 17g, see also Fig. 12) and closer to the limit.

Since [MM18] has rules only up to $n = 8$, for valence $n = 9$ Fig. 18, we choose [MM19] as a typical representative of tuned and classic subdivision. Convex input nets result in visible ripples, see Fig. 18c. The two types of saddles yield kinks in the transition to the first subdivision ring, see Fig. 18g,k. EG subdivision shows no such oscillations or kinks in Fig. 18d,h and only mild oscillations in Fig. 18l. For valence $n = 10$, Fig. 19 has four ridges elevated from the plane. While Catmull-Clark subdivision exhibits the typical pinching of highlight lines in the vicinity of the limit point Fig. 19e, EG subdivision handles the challenge well both globally and near the limit point. The example illustrates how complex examples obscure shape flaws (and are therefore not shown) since the comparison of Fig. 19c to d barely shows the difference.

Fig. 20 demonstrates that EG subdivision fares well when raising

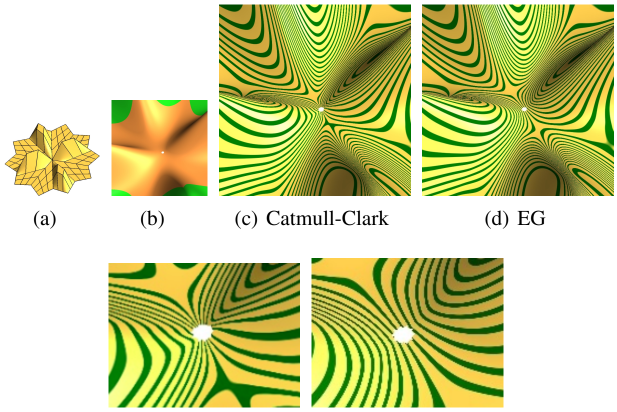

(a) (b) (c) Catmull-Clark (d) EG

(e) CC, zoom (f) EG, zoom

Figure 19: *$n = 10$ extended* **c***-net and layout (CC=Catmull-Clark).*

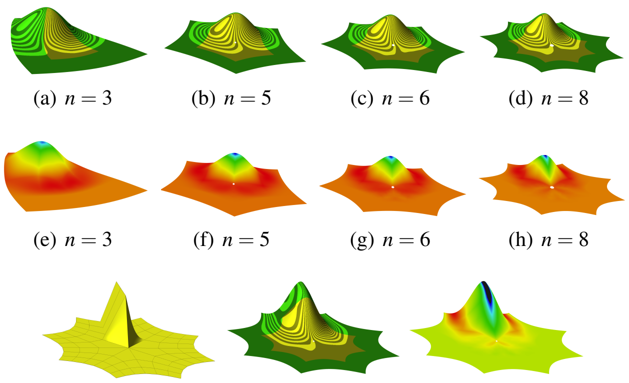

(a) $n = 3$ (b) $n = 5$ (c) $n = 6$ (d) $n = 8$

(e) $n = 3$ (f) $n = 5$ (g) $n = 6$ (h) $n = 8$

(i) $n = 8$, ridge raised

Figure 20: *Top two rows: single off-center* **c***-net node raised (top row: highlight lines, middle row: mean curvature). (bottom) entire ridge raised.*

a single **c**-net off-center point (a–h) or even a whole ridge of points (i).

It is is possible to construct a variant of EG subdivision that uses 2×2 bi-3 patches in place of each bi-4 patch of EG subdivision. The overall shape and highlight line distribution of this variant is very similar to the original so that we illustrate the differences via the uniformity of curvature after zoom to inner rings in Fig. 21. Given the fragmentation of curvature and a quadrupling of the number of patches the bi-cubic variant does not seem to provide an advantage and so is not discussed here.

Limitations: Given the structural similarity to Catmull-Clark subdivision, the main drawback is the increase of the degree to bi-4 and the concomitant heterogeneity of degree if the regular parts of the control net are interpreted as bi-3 splines, as for Catmull-Clark subdivision.

In general, for engineering analysis, subdivision surfaces combine the advantages of parametric refinability, relatively low degree

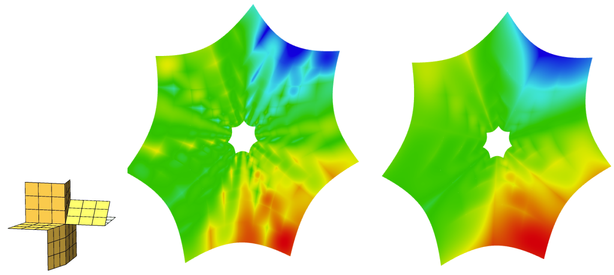

(a) $n = 7$ (b) 2×2 bi-3 variant (c) EG subdivision

Figure 21: *Mean curvature of a 2×2 bi-3 variant of EG subdivision compared to (1×1) bi-4 EG subdivision.*

and smoothness. Many alternative surface constructions, such as G-splines, rational blending constructions and manifold constructions [Pet96, YZ04, GH95, SV18] lack built-in refinability, or are of too high a degree for many applications, or are not compatible with surface exchange standards. Conversely, an inherent disadvantage of subdivision is the definition of infinitely many pieces near extraordinary points. This complicates the numerical treatment of extraordinary neighborhoods: for example, integration of derivatives across the extraordinary point requires careful estimates.

To date there exists no agreed-upon measure defining aesthetically pleasing shapes. Rather, designers characterize good shape as the absence of flaws. Flaws include oscillations, unwanted rapid changes, and non-uniform distribution of the surface highlight lines, see e.g. [Aut19, Aut22]. An unavoidable limitation is therefore that there is no 'proof' of good shape other than demonstrating the subdivision for a gallery of challenging input control nets. Obtaining good highlight line distributions for all configurations of [KP] gives hope that EG subdivision is suitable for industrial outer surface design, especially when filling the remaining hole, after a finite number of subdivision rings have been generated, by a minuscule polynomial cap.

8. Conclusion

Empirically, the new EG subdivision generates surfaces with desirably uniform highlight line distributions. Compared to other explicit subdivision algorithms, EG subdivision keeps shape oscillations under control by following a sequence of evolving guide surfaces. In contrast to the static, initial guide of Guided Subdivision, these evolving surfaces are baked into and part of the EG subdivision rules.

Thanks to these evolving guides, starting with the first step, EG subdivision surfaces join gracefully to the surrounding surfaces. Ma-Ma and similar rules focus on limit behaviour and not the initial transition. Formally, the limit curvature of [MM18, MM19] is bounded, but since the formulas in both papers were presented with 4 digit accuracy, their μ differs from λ^2, albeit slightly less than for EG subdivision. Yet the EG subdivision highlight line distribution near the center is more uniform and straight than for Ma-Ma. This illustrates that eigenanalysis, while relevant, does not determine good shape.

EG subdivision is associated with a **d**-net stemming from C^2 bi-4 splines. However, there is an easy initial step, namely applying the matrix **R**, to start EG subdivision from a **c**-net, the net configuration of Catmull-Clark subdivision. A Catmull-Clark subdivision surface 'cap' can therefore be replaced by a EG subdivision cap near extraordinary points. We can therefore interpret regular subnets as uniform bi-3 splines that smoothly join the surface caps generated by EG subdivision, see [LKP22]. A control-net modeling session with EG subdivision then looks like a modeling session with Catmull-Clark.

EG subdivision uses five special subdivision rules in addition to the once-executed rule for $\mathbf{c_0}$. The central extraordinary limit point $\mathbf{c_0}$ is computed at the beginning and remains fixed throughout EG subdivision. The footprint of the five special rules is smaller than that of guided subdivision but sufficiently large to result in good highlight line distributions. Although the derivation of the EG rules is non-trivial, the implementation, see [LKP22], amounts to applying the subdivision matrices $\mathbf{A}_n$ to the **d**-net. The matrices $\mathbf{A}_n$ are defined by the arrays given Section 5 and the Appendix. Rules for $n > 10$ exist, but such designs are not encouraged since high valence is better modeled by polar configurations, see e.g. [MP09]. Just as for classical subdivision, the vector of $12n+1$ entries representing the $12n$ nodes of the current **d**-net plus the central point $\mathbf{c_0}$ is multiplied by the subdivision matrix to obtain the finer control net near the extraordinary point. That is, the implementation only differs from Catmull-Clark code by computing the matrix-vector product $\mathbf{A}_n\mathbf{d}$ in place of the sparser product of Catmull-Clark subdivision that is often implemented via stencils. For $n \le 10$, switching from Catmull-Clark to EG subdivision no more than doubles the execution time of the surface cap. Various GPU implementation strategies used for Catmull-Clark subdivision can, in the future, be adapted to EG subdivision.

References

[ADS06] AUGSDÖRFER U. H., DODGSON N. A., SABIN M. A.: Tuning subdivision by minimising gaussian curvature variation near extraordinary vertices. *Computer Graphics Forum 25*, 3 (2006), 263–272. 2

[Aut19] AUTODESK: Surface evaluation – iso angle and iso curves, 2019. Apr07. URL: http://help.autodesk.com/view/ALIAS/2015/ENU/?guid=GUID-2FCE06EB-8EF7-4507-92F7-82A73A0DF378. 10

[Aut22] AUTODESK: Theory builder, introduction to class-a, 2022. accessed Nov 22. URL: https://www.aliasworkbench.com/theoryBuilders/TB11_class_a.htm. 10

[BC94] BEIER K.-P., CHEN Y.: Highlight-line algorithm for realtime surface-quality assessment. *Comp-Aid Design 26*, 4 (1994), 268–277. 1

[CADS09] CASHMAN T. J., AUGSDÖRFER U. H., DODGSON N. A., SABIN M. A.: NURBS with extraordinary points: high-degree, non-uniform, rational subdivision schemes. *ACM Tr Graph 28*, 3 (2009), 46:1–46:9. 2

[CC78] CATMULL E., CLARK J.: Recursively generated B-spline surfaces on arbitrary topological meshes. *Computer-Aided Design 10* (Sept. 1978), 350–355. 1, 2, 3

[dB87] DE BOOR C.: B-form basics. In *Geometric Modeling: Algorithms and New Trends* (1987), Farin G., (Ed.), SIAM, pp. 131–148. 4

[DKT98] DEROSE T., KASS M., TRUONG T.: Subdivision surfaces in character animation. In *Proceedings of the 25th annual conference on Computer graphics and interactive techniques* (1998), pp. 85–94. 2

[Far88] FARIN G.: *Curves and Surfaces for Computer Aided Geometric Design: A Practical Guide*. Academic Press, 1988. 4

[GH95] GRIMM C. M., HUGHES J. F.: Modeling surfaces of arbitrary topology using manifolds. In *Proceedings of the 22nd annual conference on Computer graphics and interactive techniques* (1995), pp. 359–368. 10

[HKD93] HALSTEAD M., KASS M., DEROSE T.: Efficient, fair interpolation using catmull-clark surfaces. In *Proceedings of the 20th annual conference on Computer graphics and interactive techniques, Siggraph 1993* (New York, NY, USA, Aug. 1993), Valastyan L., Walsh L., (Eds.), ACM Press, pp. 35–44. 4

[KP] KARČIAUSKAS K., PETERS J.: Quad-net obstacle course. http://www.cise.ufl.edu/research/SurfLab/shape_gallery.shtml. Accessed: March 2022. 10

[KP07] KARČIAUSKAS K., PETERS J.: Concentric tesselation maps and curvature continuous guided surfaces. *Computer Aided Geometric Design 24*, 2 (Feb 2007), 99–111. 2

[KP15] KARČIAUSKAS K., PETERS J.: Can bi-cubic surfaces be class A? *Computer Graphics Forum 34*, 5 (August 2015), 229–238. 4

[KP18] KARČIAUSKAS K., PETERS J.: Refinable bi-quartics for design and analysis. *Computer-Aided Design* (2018), 1–10. 2, 3, 5

[KP19] KARČIAUSKAS K., PETERS J.: Curvature-bounded guided subdivision: biquartics vs bicubics. *Computer Aided Design* (Jul 2019), 1–11. 2, 3, 8

[KPR04] KARCIAUSKAS K., PETERS J., REIF U.: Shape characterization of subdivision surfaces – case studies. *Computer-Aided Geometric Design 21*, 6 (july 2004), 601–614. 2

[LFS16] LI X., FINNIGAN G., SEDERBERG T.: G^1 non-uniform Catmull-Clark surfaces. *ACM Transactions on Graphics 35* (07 2016), 1–8. 1, 2

[LKP22] LO K., KARČIAUSKAS K., PETERS J.: Eg_Refine reference implementation, 2022. Dec 10. URL: https://bitbucket.org/surflab/eg_refine. 6, 11

[Ma05] MA W.: Subdivision surfaces for cad—an overview. *Computer-Aided Design 37*, 7 (2005), 693–709. 2

[MM18] MA Y., MA W.: Subdivision schemes with optimal bounded curvature near extraordinary vertices. *Computer Graphics Forum 37*, 7 (Oct 2018), 455–467. 1, 2, 3, 8, 9, 10

[MM19] MA Y., MA W.: Subdivision schemes for quadrilateral meshes with the least polar artifact in extraordinary regions. *Comput. Graph. Forum 38*, 7 (2019), 127–139. 3, 9, 10

[MP09] MYLES A., PETERS J.: Bi-3 c 2 polar subdivision. *ACM Transactions on Graphics (TOG) 28*, 3 (2009), 1–12. 11, 12

[NLMD12] NIESSNER M., LOOP C., MEYER M., DEROSE T.: Feature-adaptive gpu rendering of catmull-clark subdivision surfaces. *ACM Transactions on Graphics (TOG) 31*, 1 (2012), 1–11. 1, 2

[Pet96] PETERS J.: Curvature continuous spline surfaces over irregular meshes. *Computer Aided Geometric Design 13*, 2 (1996), 101–131. 10

[PR08] PETERS J., REIF U.: *Subdivision Surfaces*, vol. 3 of *Geometry and Computing*. Springer-Verlag, New York, 2008. 3

[PU98] PRAUTZSCH H., UMLAUF G.: A g 2-subdivision algorithm. In *Geometric Modelling*. Springer, 1998, pp. 217–224. 1

[Sab91] SABIN M. A.: Cubic recursive division with bounded curvature. In *Curves and surfaces*. Elsevier, 1991, pp. 411–414. 1

[SV18] SALVI P., VÁRADY T.: Multi-sided Bézier surfaces over concave polygonal domains. *Comput. Graph 74* (2018), 56–65. 10

[WLZH21] WEI X., LI X., ZHANG Y. J., HUGHES T. J.: Tuned hybrid nonuniform subdivision surfaces with optimal convergence rates. *International Journal for Numerical Methods in Engineering 122*, 9 (2021), 2117–2144. 2

[YZ04] YING L., ZORIN D.: A simple manifold-based construction of surfaces of arbitrary smoothness. *ACM Transactions on Graphics (TOG) 23*, 3 (2004), 271–275. 10

[ZSC18] ZHANG Q., SABIN M., CIRAK F.: Subdivision surfaces with isogeometric analysis adapted refinement weights. *Computer-Aided Design 102* (2018), 104–114. 2

Appendix: The arrays for $n = 6, 7, 8, 9, 10$

Valences higher than $n = 10$ are best modeled using polar configurations [MP09]. Recall that the entries are scaled by 10^5, i.e. are numbers of absolute value less than 1.

For $n = 6$,

$$A^6_{11} := \begin{pmatrix} 195 & -490 & 623 & -140 & -490 & 4810 & 4137 & 3117 & 623 & 4137 & 63933 & 7100 \\ 342 & -398 & 60 & 165 & -643 & 153 & 349 & -750 & 355 & 342 & -796 & 481 \\ 222 & -262 & -41 & 121 & -345 & -124 & 704 & -157 & 27 & 807 & -968 & -641 \\ 27 & 10 & -126 & 121 & 10 & -257 & 354 & -157 & -126 & 354 & -241 & -641 \end{pmatrix}$$

$$A^6_{22} := \begin{pmatrix} 691 & -1154 & 1518 & -88 & -1154 & 1397 & -5589 & -2697 & 1518 & -5589 & 44242 & 15443 \\ 1107 & -1155 & 80 & 540 & -2274 & 641 & 1058 & -2136 & 1210 & 1852 & 1130 & -54 \\ 585 & -609 & -304 & 305 & -924 & -575 & 2575 & 519 & -66 & 3057 & -5551 & -4453 \\ -348 & 729 & -717 & 305 & 729 & -1152 & 695 & 519 & -717 & 695 & -1356 & -4453 \end{pmatrix}$$

$$A^6_{21} := \begin{pmatrix} 409 & -852 & 852 & -6 & -394 & 421 & 5574 & 2189 & 686 & -3575 & 49782 & 25832 \\ 527 & -545 & 146 & 287 & -1117 & 491 & -306 & -1681 & 561 & 1785 & 4561 & 1936 \\ 615 & -738 & -55 & 263 & -1047 & -101 & 1899 & -344 & 245 & 2081 & -3384 & -1918 \\ -83 & 195 & -249 & 113 & 261 & -540 & 330 & 326 & -364 & 510 & -311 & -1452 \\ 131 & -99 & -249 & 327 & -126 & -431 & 1134 & -881 & -152 & 846 & -1571 & -1306 \\ 715 & -1327 & 596 & -59 & -820 & 130 & 1558 & -394 & -10 & 1625 & -2372 & 5053 \end{pmatrix}$$

$$A^6_{31} := \begin{pmatrix} 508 & -1059 & 900 & -93 & -620 & 727 & 627 & 5908 & 110 & 265 & 14832 & 49296 \\ 508 & -620 & 110 & 363 & -1059 & 727 & 265 & -2727 & 900 & 627 & 14832 & 3395 \\ 696 & -794 & -57 & 310 & -1262 & 14 & 1852 & -568 & 405 & 2036 & -2474 & -1968 \\ -4 & 95 & -258 & 119 & 128 & -560 & 670 & 480 & -353 & 923 & -1326 & -2000 \end{pmatrix}$$

$$A^6_{32} := \begin{pmatrix} 781 & -1843 & 1572 & -12 & -773 & 1255 & -1663 & -4879 & 256 & -1014 & 9893 & 34152 \\ 781 & -773 & 256 & 463 & -1843 & 1255 & -1014 & -3816 & 1572 & -1663 & 9893 & 4992 \\ 1200 & -1288 & -227 & 516 & -2277 & 9 & 3563 & -392 & 875 & 3395 & -5835 & -5458 \\ -303 & 620 & -648 & 101 & 701 & -1205 & 964 & 1841 & -865 & 1509 & -3393 & -5397 \end{pmatrix}$$

For $n = 7$,

$$A^7_{11} := \begin{pmatrix} 1649 & -2653 & 1079 & 712 & -2653 & 6369 & 5384 & 403 & 1079 & 5384 & 62604 & 8301 \\ 1305 & -1557 & 38 & 763 & -1997 & -61 & 2516 & -2607 & 387 & 2676 & -2787 & 1537 \\ 420 & -446 & -101 & 185 & -601 & -234 & 1218 & -147 & -113 & 1350 & -1171 & -781 \\ -93 & 174 & -103 & -45 & 246 & -290 & -43 & 616 & -233 & 21 & 185 & -918 \end{pmatrix}$$

$$A^7_{22} := \begin{pmatrix} 5832 & -8101 & 2137 & 3660 & -8101 & 798 & 5305 & -15649 & 2137 & 5305 & 35906 & 21029 \\ 3961 & -4574 & 95 & 1995 & -6317 & 4 & 7442 & -6686 & 988 & 8899 & -3417 & 3345 \\ 521 & -282 & -432 & -239 & -864 & -670 & 2423 & 2810 & -496 & 2936 & -4147 & -5538 \\ -1449 & 2086 & -415 & -1131 & 2395 & -880 & -2497 & 5701 & -946 & -2245 & 1336 & -5879 \end{pmatrix}$$

$$A^7_{21} := \begin{pmatrix} 2885 & -4258 & 990 & 2256 & -3619 & 65 & 11354 & -5554 & 1006 & 1426 & 45673 & 29166 \\ 2545 & -3097 & 233 & 1471 & -3911 & 76 & 4356 & -5514 & 399 & 7121 & 151 & 4283 \\ 877 & -854 & -246 & 329 & -1442 & -296 & 2477 & -181 & -7 & 2714 & -2638 & -1977 \\ -319 & 430 & -119 & -318 & 683 & -452 & -208 & 1870 & -530 & -23 & -425 & -2056 \\ -543 & 919 & -324 & -161 & 844 & -441 & -1104 & 1397 & -212 & -1150 & 1571 & -2120 \\ 19 & 114 & -458 & 729 & 30 & -421 & 928 & -1861 & -138 & 696 & -1557 & -451 \\ 1502 & -2449 & 429 & 1395 & -1616 & -172 & 3382 & -5219 & -161 & 3370 & -2822 & 7200 \end{pmatrix}$$

$$A^7_{31} := \begin{pmatrix} 2541 & -3792 & 872 & 2000 & -3280 & 190 & 5492 & -1538 & 103 & 5818 & 10039 & 54445 \\ 2541 & -3280 & 103 & 1738 & -3792 & 190 & 5818 & -7146 & 872 & 5492 & 10039 & 5391 \\ 1058 & -1080 & -179 & 410 & -1758 & -193 & 2573 & -666 & 93 & 2892 & -1732 & -1305 \\ -278 & 425 & -151 & -358 & 538 & -399 & -50 & 2079 & -465 & 153 & -868 & -2504 \\ -692 & 1077 & -287 & -358 & 1077 & -415 & -1368 & 2079 & -287 & -1368 & 1410 & -2504 \end{pmatrix}$$

$$A^7_{32} := \begin{pmatrix} 5498 & -8345 & 1585 & 4853 & -6921 & 304 & 10167 & -22235 & 490 & 10813 & -1236 & 44864 \\ 5498 & -6921 & 490 & 3294 & -8345 & 304 & 10813 & -13424 & 1585 & 10167 & -1236 & 10408 \\ 1937 & -1799 & -448 & 449 & -3428 & -328 & 4891 & 278 & 438 & 4874 & -3772 & -4503 \\ -1285 & 1837 & -387 & -1403 & 2101 & -825 & -1425 & 6914 & -1137 & -935 & -1786 & -7449 \\ -2288 & 3411 & -716 & -1403 & 3411 & -865 & -4596 & 6914 & -716 & -4596 & 3658 & -7449 \end{pmatrix}$$

For $n = 8$,

$$A^8_{11} := \begin{pmatrix} 3170 & -4510 & 920 & 1956 & -4510 & 6628 & 7736 & -2189 & 920 & 7736 & 61019 & 8736 \\ 2083 & -2333 & -209 & 1181 & -2807 & -798 & 4581 & -3462 & -29 & 4678 & -3918 & 1918 \\ 112 & -11 & -139 & -67 & -227 & -130 & 520 & 622 & -219 & 489 & -101 & -1145 \\ -264 & 309 & -34 & -105 & 477 & -110 & -461 & 680 & -193 & -421 & 209 & -763 \\ 47 & 38 & -68 & -105 & 38 & -292 & 71 & 680 & -68 & 71 & 113 & -763 \end{pmatrix}$$

$$A^8_{22} := \begin{pmatrix} 10373 & -12886 & 575 & 8227 & -12886 & -3151 & 16663 & -25704 & 575 & 16663 & 30076 & 22718 \\ 6054 & -6715 & -524 & 2897 & -8311 & -2184 & 13246 & -8565 & -600 & 14241 & -5536 & 4705 \\ -666 & 1221 & -285 & -1440 & 469 & 86 & -611 & 5615 & -563 & -718 & 217 & -5930 \\ -2095 & 2510 & 68 & -1699 & 3042 & 205 & -4251 & 6254 & -468 & -4122 & 1359 & -4999 \\ -1137 & 1693 & -49 & -1699 & 1693 & -375 & -2643 & 6254 & -49 & -2643 & 1084 & -4999 \end{pmatrix}$$

$$A^8_{21} := \begin{pmatrix} 4909 & -6314 & 17 & 4907 & -5735 & -1787 & 16674 & -11343 & 425 & 6455 & 43020 & 30282 \\ 4130 & -4760 & -272 & 2463 & -5448 & -1527 & 8827 & -7586 & -680 & 11662 & -2629 & 4990 \\ 470 & -260 & -237 & -274 & -903 & -222 & 1431 & 1425 & -261 & 1325 & -355 & -2179 \\ -1018 & 1213 & -32 & -619 & 1430 & 157 & -1901 & 2455 & -304 & -1845 & 583 & -2274 \\ -171 & 236 & 8 & -280 & 463 & -322 & -478 & 1283 & -120 & -430 & 307 & -984 \\ -375 & 750 & -198 & -611 & 415 & -205 & -756 & 2467 & 30 & -829 & 372 & -2550 \\ -802 & 1013 & -320 & 488 & 1036 & 151 & -1316 & -1067 & -98 & -1328 & 399 & -310 \\ 1686 & -2496 & -51 & 2896 & -1690 & -635 & 3551 & -8287 & -280 & 3936 & -1872 & 7579 \end{pmatrix}$$

$$A^8_{31} := \begin{pmatrix} 3675 & -4738 & 38 & 3873 & -4401 & -1343 & 8558 & -5588 & -532 & 9748 & 8074 & 56324 \\ 3675 & -4401 & -532 & 2740 & -4738 & -1343 & 9748 & -9017 & 38 & 8558 & 8074 & 5459 \\ 866 & -784 & -187 & 16 & -1374 & -328 & 2138 & 330 & -273 & 2162 & -130 & -1074 \\ -860 & 1077 & -32 & -714 & 1122 & 178 & -1585 & 2657 & -234 & -1563 & 469 & -2399 \\ -501 & 621 & 34 & -526 & 825 & -106 & -1129 & 1980 & -108 & -1084 & 431 & -1470 \end{pmatrix}$$

$$A^8_{32} := \begin{pmatrix} 9036 & -11741 & -575 & 10319 & -10636 & -3489 & 20136 & -34655 & -909 & 21657 & -7903 & 49585 \\ 9036 & -10636 & -909 & 6047 & -11741 & -3489 & 21657 & -19408 & -575 & 20136 & -7903 & 11910 \\ 1787 & -1489 & -389 & -501 & -3016 & -608 & 4490 & 2410 & -288 & 3596 & -167 & -3650 \\ -2779 & 3468 & 9 & -2521 & 3555 & 730 & -5353 & 8857 & -514 & -5301 & 1515 & -7416 \\ -1996 & 2461 & 180 & -2111 & 2969 & 46 & -4464 & 7358 & -187 & -4352 & 1495 & -5223 \end{pmatrix}$$

For $n = 9$,

$$A^9_{11} := \begin{pmatrix} 4093 & -5443 & 535 & 2924 & -5443 & 6544 & 9053 & -3513 & 535 & 9053 & 60551 & 8408 \\ 2689 & -2873 & -538 & 1577 & -3251 & -1631 & 6281 & -4215 & -524 & 6180 & -4560 & 2304 \\ -68 & 197 & -36 & -491 & -53 & 40 & 40 & 1541 & -202 & -256 & 675 & -1322 \\ -740 & 825 & 67 & -308 & 932 & 343 & -1654 & 1150 & 5 & -1587 & 812 & -1033 \\ 235 & -241 & -97 & 279 & -114 & -376 & 505 & -409 & -100 & 616 & -389 & -22 \end{pmatrix}$$

$$A^9_{22} := \begin{pmatrix} 12251 & -14026 & -1298 & 11142 & -14026 & -6557 & 21567 & -29660 & -1298 & 21567 & 29964 & 21461 \\ 7408 & -7911 & -1396 & 3947 & -9024 & -4402 & 17317 & -10685 & -2139 & 17532 & -6277 & 5988 \\ -853 & 1312 & 120 & -2450 & 545 & 584 & -1356 & 7126 & -397 & -2273 & 2175 & -5230 \\ -3200 & 3597 & 500 & -2351 & 3859 & 1682 & -7161 & 7197 & 282 & -7028 & 2802 & -5147 \\ -685 & 856 & 71 & -836 & 1201 & -225 & -1625 & 3205 & 47 & -1331 & -481 & -2550 \end{pmatrix}$$

$$A^9_{21} := \begin{pmatrix} 5670 & -6637 & -990 & 6444 & -6194 & -3310 & 18807 & -13281 & -318 & 8488 & 43022 & 29636 \\ 4821 & -5263 & -929 & 3259 & -5708 & -2923 & 11101 & -8858 & -1709 & 13818 & -3350 & 5199 \\ 588 & -430 & -131 & -642 & -952 & -318 & 1665 & 1930 & -398 & 1080 & 381 & -1623 \\ -1649 & 1879 & 237 & -1245 & 1901 & 942 & -3629 & 3738 & 104 & -3671 & 1743 & -2714 \\ -409 & 425 & 15 & 52 & 705 & -12 & -1005 & 296 & 8 & -760 & 73 & -483 \\ 504 & -409 & -129 & -235 & -473 & -645 & 1191 & 1056 & -126 & 1136 & -906 & -977 \\ -887 & 1213 & 56 & -1294 & 946 & 346 & -1841 & 3811 & 96 & -2058 & 681 & -2783 \\ -1253 & 1333 & -12 & 487 & 1499 & 759 & -2874 & -1213 & 174 & -2642 & 1646 & 357 \\ 2065 & -2663 & -443 & 3870 & -2077 & -1211 & 4092 & -9471 & -401 & 5004 & -1701 & 7073 \end{pmatrix}$$

$$A^9_{31} := \begin{pmatrix} 3781 & -4394 & -596 & 4535 & -4250 & -2346 & 8932 & -6027 & -1133 & 10845 & 8383 & 56431 \\ 3781 & -4250 & -1133 & 3257 & -4394 & -2346 & 10845 & -9453 & -596 & 8932 & 8383 & 4984 \\ 968 & -922 & -180 & -83 & -1319 & -546 & 2425 & 312 & -489 & 2119 & 319 & -452 \\ -1104 & 1292 & 179 & -1095 & 1222 & 652 & -2385 & 3199 & 50 & -2505 & 1209 & -2244 \\ -708 & 779 & 103 & -418 & 953 & 268 & -1636 & 1441 & 75 & -1495 & 393 & -1091 \\ 19 & 72 & -16 & -418 & 72 & -253 & 61 & 1441 & -16 & 61 & -451 & -1091 \end{pmatrix}$$

$$A^9_{32} := \begin{pmatrix} 9998 & -11695 & -2527 & 13001 & -11040 & -6386 & 23394 & -37999 & -2496 & 25842 & -8658 & 49843 \\ 9998 & -11040 & -2496 & 7824 & -11695 & -6386 & 25842 & -21926 & -2527 & 23394 & -8658 & 11595 \\ 2395 & -2253 & -396 & -586 & -3331 & -1303 & 6050 & 1746 & -821 & 4129 & 724 & -1650 \\ -3362 & 3927 & 610 & -3571 & 3710 & 2020 & -7294 & 10249 & 242 & -7655 & 3389 & -6935 \\ -2551 & 2840 & 453 & -1977 & 3278 & 1132 & -5850 & 6153 & 360 & -5504 & 1356 & -4230 \\ -716 & 1064 & 145 & -1977 & 1064 & -200 & -1575 & 6153 & 145 & -1575 & -828 & -4230 \end{pmatrix}$$

For $n = 10$,

$$A^{10}_{11} := \begin{pmatrix} 4415 & -5674 & 258 & 3428 & -5674 & 6674 & 9056 & -3686 & 258 & 9056 & 60949 & 7690 \\ 3115 & -3194 & -903 & 2119 & -3464 & -2354 & 7453 & -5254 & -938 & 7248 & -4866 & 2746 \\ 166 & -75 & -25 & -594 & -309 & -98 & 617 & 1548 & -265 & 42 & 671 & -1019 \\ -1079 & 1156 & 265 & -803 & 1171 & 781 & -2506 & 2208 & 216 & -2521 & 1201 & -1460 \\ -146 & 154 & -44 & 320 & 289 & -50 & -445 & -454 & 18 & -174 & -13 & -72 \\ 668 & -619 & -243 & 320 & -619 & -732 & 1594 & -454 & -243 & 1594 & -865 & -72 \end{pmatrix}$$

$$A^{10}_{22} := \begin{pmatrix} 12317 & -13272 & -2483 & 12345 & -13272 & -8251 & 21587 & -29645 & -2483 & 21587 & 32596 & 19201 \\ 8111 & -8335 & -2296 & 5324 & -9055 & -6061 & 19425 & -13318 & -3228 & 19270 & -6145 & 7100 \\ 123 & 133 & 98 & -2248 & -512 & 24 & 952 & 5692 & -576 & -647 & 1762 & -3437 \\ -3592 & 3859 & 1008 & -3392 & 3853 & 2649 & -8248 & 8942 & 819 & -8409 & 3342 & -5447 \\ -1618 & 1739 & 329 & -886 & 2055 & 811 & -3944 & 3070 & 456 & -3324 & 404 & -2426 \\ 311 & -86 & -149 & -886 & -86 & -825 & 887 & 3070 & -149 & 887 & -1713 & -2426 \end{pmatrix}$$

$$A^{10}_{21} := \begin{pmatrix} 5610 & -6140 & -1586 & 6933 & -5793 & -4017 & 18722 & -12896 & -796 & 8274 & 44253 & 28456 \\ 4889 & -5085 & -1437 & 3863 & -5357 & -3702 & 11542 & -9617 & -2354 & 14279 & -2990 & 5152 \\ 1088 & -997 & -249 & -338 & -1373 & -776 & 2895 & 862 & -608 & 1993 & 175 & -618 \\ -1609 & 1754 & 463 & -1732 & 1664 & 1228 & -3620 & 4479 & 311 & -3889 & 1792 & -2689 \\ -1056 & 1098 & 218 & -361 & 1270 & 659 & -2587 & 1267 & 287 & -2248 & 710 & -1035 \\ 524 & -491 & -220 & 429 & -403 & -667 & 1188 & -635 & -168 & 1373 & -955 & -27 \\ 172 & -12 & -57 & -824 & -158 & -369 & 606 & 2355 & -132 & 307 & -573 & -1596 \\ -1426 & 1609 & 358 & -1548 & 1494 & 1000 & -3194 & 3951 & 344 & -3394 & 1244 & -2359 \\ -960 & 900 & 66 & 999 & 1105 & 770 & -2538 & -2494 & 305 & -2011 & 1516 & 1242 \\ 2507 & -2890 & -769 & 4316 & -2501 & -1857 & 4968 & -9454 & -674 & 6178 & -1869 & 6258 \end{pmatrix}$$

$$A^{10}_{31} := \begin{pmatrix} 3419 & -3680 & -851 & 4419 & -3649 & -2696 & 8017 & -4959 & -1476 & 10394 & 9411 & 56122 \\ 3419 & -3649 & -1476 & 3442 & -3680 & -2696 & 10394 & -9235 & -851 & 8017 & 9411 & 4417 \\ 1185 & -1160 & -297 & 215 & -1406 & -859 & 2987 & -549 & -662 & 2539 & 294 & 235 \\ -851 & 950 & 269 & -1183 & 845 & 665 & -1853 & 3024 & 131 & -2136 & 1031 & -1779 \\ -973 & 1028 & 250 & -697 & 1105 & 665 & -2301 & 1947 & 260 & -2168 & 678 & -1261 \\ -89 & 130 & -6 & -129 & 197 & -96 & -228 & 598 & 26 & -91 & -349 & -557 \end{pmatrix}$$

$$A^{10}_{32} := \begin{pmatrix} 9504 & -10305 & -3546 & 13468 & -9935 & -7648 & 22629 & -36623 & -3506 & 25599 & -6951 & 48820 \\ 9504 & -9935 & -3506 & 8685 & -10305 & -7648 & 25599 & -22321 & -3546 & 22629 & -6951 & 10611 \\ 3259 & -3193 & -783 & 432 & -3887 & -2331 & 8236 & -1160 & -1317 & 5785 & 504 & 521 \\ -2594 & 2889 & 857 & -3763 & 2575 & 2036 & -5635 & 9556 & 441 & -6482 & 2887 & -5520 \\ -3213 & 3413 & 890 & -2737 & 3600 & 2240 & -7526 & 7386 & 888 & -7221 & 2048 & -4542 \\ -979 & 1148 & 235 & -1302 & 1324 & 285 & -2289 & 3999 & 313 & -1939 & -685 & -2784 \end{pmatrix}$$